

Comparison of the MSMS and NanoShaper molecular surface triangulation codes in the TABI Poisson–Boltzmann solver

Leighton Wilson*, Robert Krasny†

October 22, 2020

Abstract

The Poisson-Boltzmann (PB) implicit solvent model is a popular framework for studying the electrostatics of biomolecules immersed in water with dissolved salt. In this model the dielectric interface between the biomolecule and solvent is often taken to be the molecular surface or solvent-excluded surface (SES), and the quality of the SES triangulation is critical in boundary element simulations of the PB model. In this work we compare the MSMS and NanoShaper surface triangulation codes for a set of 38 biomolecules. While MSMS produces triangles of exceedingly small area and large aspect ratio, the two codes yield comparable values for the SES surface area and electrostatic solvation energy, where the latter calculations were performed using the treecode-accelerated boundary integral (TABI) PB solver. However we found that Nanoshaper is more efficient and reliable than MSMS, especially when parameters are set to produce highly resolved triangulations.

Keywords: solvated biomolecule, solvent excluded surface, electrostatics, Poisson–Boltzmann, boundary element method, treecode ■

*Department of Mathematics, University of Michigan, Ann Arbor, MI 48109

†Department of Mathematics, University of Michigan, Ann Arbor, MI 48109

INTRODUCTION

Implicit solvent models play a key role in computational modeling of electrostatic interactions between biomolecules and their solvent environment^{1–3}. Of particular importance is the Poisson–Boltzmann (PB) implicit solvent model^{4,5}. Figure 1 shows the interior domain $\Omega_1 \subset \mathbb{R}^3$ containing the solute biomolecule, the exterior domain $\Omega_2 = \mathbb{R}^3 \setminus \overline{\Omega}_1$ containing the ionic solvent, and the dielectric interface $\Gamma = \overline{\Omega}_1 \cap \overline{\Omega}_2$. In a 1:1 electrolyte at low ionic concentration, one can utilize the linearized PB equation for the electrostatic potential ϕ ,

$$-\nabla \cdot (\varepsilon(\mathbf{x})\nabla\phi(\mathbf{x})) + \bar{\kappa}^2(\mathbf{x})\phi(\mathbf{x}) = \sum_{k=1}^{N_c} q_k \delta(\mathbf{x} - \mathbf{y}_k), \quad \mathbf{x} \in \mathbb{R}^3, \quad (1)$$

where $\varepsilon(\mathbf{x})$ is the dielectric constant, $\bar{\kappa}$ is the modified Debye–Hückel inverse length in units of \AA^{-1} , N_c is the number of atoms in the solute biomolecule, \mathbf{y}_k is the position of the k th solute atom, and q_k is the associated partial charge in units of fundamental charge e_c . The dielectric interface conditions are

$$\phi_1(\mathbf{x}) = \phi_2(\mathbf{x}), \quad \varepsilon_1 \frac{\partial\phi_1(\mathbf{x})}{\partial n} = \varepsilon_2 \frac{\partial\phi_2(\mathbf{x})}{\partial n}, \quad \mathbf{x} \in \Gamma, \quad (2)$$

where $\phi_1(\mathbf{x})$ and $\phi_2(\mathbf{x})$ are the limiting values approaching the interface Γ from inside and outside the biomolecule, respectively, and n indicates the outward normal direction on the interface. The first condition in Eq. (2) expresses continuity of the potential across the interface, and the second condition expresses continuity of the electric flux. The far-field boundary condition is

$$\lim_{|\mathbf{x}| \rightarrow \infty} \phi(\mathbf{x}) = 0. \quad (3)$$

The present work assumes that ε and $\bar{\kappa}$ are piecewise constant,

$$\varepsilon(\mathbf{x}) = \begin{cases} \varepsilon_1, & \mathbf{x} \in \Omega_1, \\ \varepsilon_2, & \mathbf{x} \in \Omega_2, \end{cases}, \quad \bar{\kappa}^2(\mathbf{x}) = \begin{cases} 0, & \mathbf{x} \in \Omega_1, \\ \left(\frac{8\pi N_A e_c^2}{1000 k_B T} \right) I_s, & \mathbf{x} \in \Omega_2, \end{cases} \quad (4)$$

where N_A is Avogadro’s number, k_B is the Boltzmann constant, T is the temperature, and I_s is the molar concentration of the ionic solvent. A key quantity of interest in analyzing protein stability is the electrostatic solvation energy,

$$E_{\text{sol}} = \frac{1}{2} \sum_{k=1}^{N_c} q_k \phi_{\text{reac}}(\mathbf{y}_k), \quad (5)$$

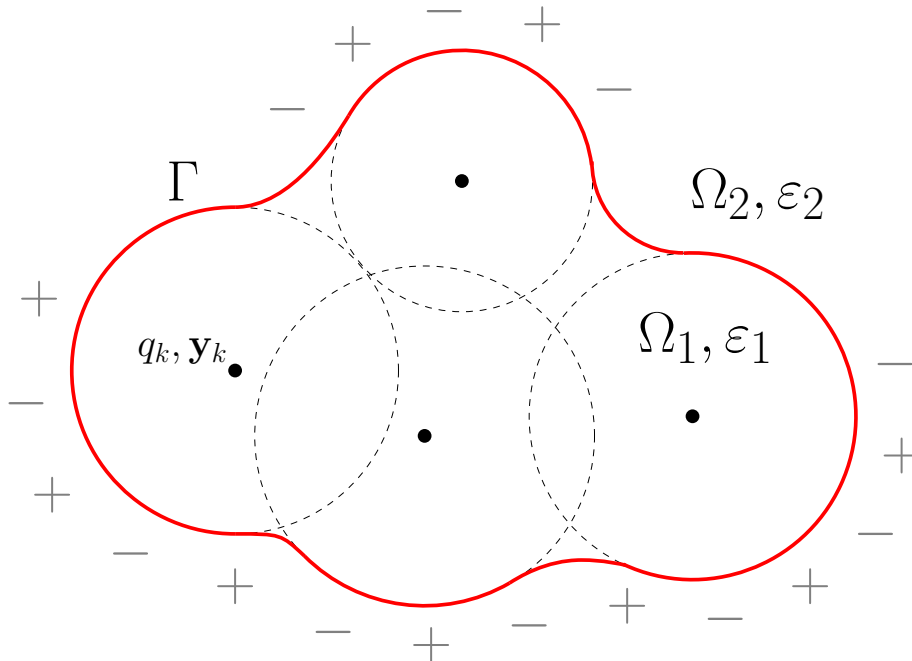


Figure 1: Poisson–Boltzmann implicit solvent model, solute domain Ω_1 with dielectric constant ε_1 , atomic charges q_k located at \mathbf{y}_k , vdW radii (dashed circles), solvent domain Ω_2 with dielectric constant ε_2 , dissolved salt ions (+, -), dielectric interface (Γ).

where the reaction field potential at an atomic position,

$$\phi_{\text{reac}}(\mathbf{y}_k) = \lim_{\mathbf{x} \rightarrow \mathbf{y}_k} \left(\phi(\mathbf{x}) - \sum_{j=1}^{N_c} \frac{q_j}{4\pi|\mathbf{x} - \mathbf{y}_j|} \right), \quad (6)$$

is the difference between the total potential and the Coulomb potential.

A variety of numerical methods have been applied to the PB model, including finite-difference^{6–13}, finite-element^{5,14,15}, and boundary element^{16–20} methods. The present work is concerned with boundary element methods (BEM) which solve for the surface potential on a triangulation of the interface; these schemes benefit from rigorous enforcement of the interface conditions and the far-field boundary condition, but they face the difficulty of evaluating singular integrals and the expense of solving a dense linear system. The treecode-accelerated boundary integral PB solver (TABI-PB¹⁹) addresses these issues using a simple collocation scheme to discretize the integrals and a treecode algorithm to reduce the cost of solving the linear system from $O(N^2)$ to $O(N \log N)$, where N is the number of triangles representing the interface.

Dielectric Interface

Several models have been used for the dielectric interface between the solute and solvent in implicit solvent simulations^{21,22}. The **van der Waals (vdW) surface**, the simplest of these models, is the union of hard spheres with vdW radii representing the atoms comprising the biomolecule. The **solvent accessible surface (SAS)** is formed by tracing the center of a probe sphere representing a water molecule rolling along the exterior of the vdW surface; the SAS surface is equivalent to a vdW surface in which the vdW radii are increased by the probe sphere radius. The **solvent excluded surface (SES)** is formed by the inward facing surface of the probe sphere rolling along the vdW surface^{23,24}. The SES surface is comprised of spherical contact patches where the probe sphere touches the vdW surface, and toroidal reentrant patches formed by the inward facing surface of the probe sphere when it does not touch the vdW surface, i.e., when it is in contact with more than one solute atom. The **skin surface**²⁵⁻²⁷ is comprised of spherical and hyperboloid patches constructed from a set of spheres through shrinking and convex combinations. The **Gaussian surface**²⁸ is the level set of a linear combination of Gaussian functions centered at the solute atoms.

Several algorithms have been developed for triangulating these surfaces, where the input is the location and radii of the solute atoms and the output is a list of triangles that triangulate the surface. An alternative approach uses a level-set representation of the surface in an adaptive Cartesian grid^{29,30}. Publicly available surface triangulation codes include MSMS³¹, EDTSurf^{32,33}, TMSmesh^{21,28}, and NanoShaper³⁴. Previous work investigated the performance of SES surfaces and skin surfaces in the finite-difference Delphi code³⁴, and the performance of Gaussian surfaces relative to SES surfaces in the boundary element fast multipole code AFMPB³⁵. The present work focuses on the SES surface and compares the performance of MSMS and NanoShaper in computing the surface area and electrostatic solvation energy within the boundary element TABI-PB framework.

MSMS

MSMS, introduced by Sanner in 1995³¹, has gained widespread popularity for generating SES surface triangulations. After creating an analytical representation of the surface, the

algorithm generates a triangulation of specified density by fitting predefined triangulated patches to the surface. The mesh resolution is controlled by the user-specified density parameter d that sets the number of triangles in the triangulation of a given surface in units of vertices/angstrom².

NanoShaper

NanoShaper, introduced by Decherchi and Rocchia in 2012²², implements the SES surface as well as several alternatives including the Gaussian and skin surfaces. In constructing an SES surface triangulation, NanoShaper first builds a description of the surface with a set of patches, analytically if possible or else with an approximation. The code then employs a ray-casting algorithm in which rays parallel to the coordinate axes are cast and intersections with the surface are calculated. The vertex positions of intersection are then used by the marching cubes algorithm to obtain the triangulation. The mesh resolution is controlled by the user-specified scaling parameter s that sets the inverse side length of a cubic grid cell in units of angstroms.

The SES surface triangulations are commonly used to compute molecular properties such as the surface area, electrostatic potential, and electrostatic solvation energy of biomolecules. The present work investigates the triangulations produced by MSMS and NanoShaper in terms of their effect on the accuracy and efficiency of these computations.

The TABI-PB Solver

The TABI-PB solver¹⁹ relies on a reformulation of the PB Eq. (1) developed by Juffer et al. as a coupled set of boundary integral equations for the surface potential ϕ_1 and its normal derivative $\partial\phi_1/\partial n$ on the dielectric interface¹⁷,

$$\frac{1}{2}(1 + \varepsilon)\phi_1(\mathbf{x}) = \int_{\Gamma} \left[K_1(\mathbf{x}, \mathbf{y}) \frac{\partial\phi_1(\mathbf{y})}{\partial n} + K_2(\mathbf{x}, \mathbf{y}) \phi_1(\mathbf{y}) \right] dS_{\mathbf{y}} + S_1(\mathbf{x}), \quad \mathbf{x} \in \Gamma, \quad (7a)$$

$$\frac{1}{2} \left(1 + \frac{1}{\varepsilon} \right) \frac{\partial\phi_1(\mathbf{x})}{\partial n} = \int_{\Gamma} \left[K_3(\mathbf{x}, \mathbf{y}) \frac{\partial\phi_1(\mathbf{y})}{\partial n} + K_4(\mathbf{x}, \mathbf{y}) \phi_1(\mathbf{y}) \right] dS_{\mathbf{y}} + S_2(\mathbf{x}), \quad \mathbf{x} \in \Gamma, \quad (7b)$$

where $\varepsilon = \varepsilon_1/\varepsilon_2$ is the solute/solvent ratio of dielectric constants. The kernels K_1, K_2, K_3, K_4 depend on the Coulomb and screened Coulomb potentials,

$$G_0(\mathbf{x}, \mathbf{y}) = \frac{1}{4\pi |\mathbf{x} - \mathbf{y}|}, \quad G_\kappa(\mathbf{x}, \mathbf{y}) = \frac{e^{-\kappa|\mathbf{x}-\mathbf{y}|}}{4\pi |\mathbf{x} - \mathbf{y}|}. \quad (8)$$

and the source terms are

$$S_1(\mathbf{x}) = \frac{1}{\varepsilon_1} \sum_{k=1}^{N_c} q_k G_0(\mathbf{x}, \mathbf{y}_k), \quad S_2(\mathbf{x}) = \frac{1}{\varepsilon_1} \sum_{k=1}^{N_c} q_k \frac{\partial G_0(\mathbf{x}, \mathbf{y}_k)}{\partial n_{\mathbf{x}}}. \quad (9)$$

In this context the electrostatic solvation energy in Eq. (5) is obtained from the surface potential and its normal derivative,

$$E_{\text{sol}} = \frac{1}{2} \sum_{k=1}^{N_c} q_k \int_{\Gamma} \left[K_1(\mathbf{y}_k, \mathbf{y}) \frac{\partial \phi_1(\mathbf{y})}{\partial n} + K_2(\mathbf{y}_k, \mathbf{y}) \phi_1(\mathbf{y}) \right] dS_{\mathbf{y}}. \quad (10)$$

The TABI-PB solver calculates the surface integrals using a boundary element method on the triangulated SES surface, where the collocation points are the triangle centroids. The resulting linear system for the surface potentials and their normal derivatives is solved by GMRES iteration, while a treecode algorithm is employed to accelerate the matrix-vector product in each step of the iteration¹⁹.

METHODOLOGY

To assess the SES surface triangulations produced by MSMS and NanoShaper, we compute the surface area S_a and electrostatic solvation energy E_{sol} for a test set of 38 biomolecules comprising peptides, proteins, and nucleic acid fragments, where S_a is computed by summing the areas of the triangles and E_{sol} is computed using TABI-PB. In addition to examining the accuracy of these results, we report the total CPU time for the TABI-PB computation; the CPU time for generating the triangulation and other pre-processing steps is negligible in comparison to the boundary element computation time. Surface visualizations were generated with VTK ParaView.

The biomolecules in the test set, listed in Table 1, are those with widely available PDB entries from the list used in a previous molecular surface comparison study³⁵. We generate

Table 1: PDB ID and number of atoms for test set of 38 biomolecules comprising proteins, peptides, and nucleic acid fragments³⁵.

Index	1	2	3	4	5	6	7	8
PDB ID	2LWC	1GNA	1S4J	1CB3	1V4Z	1BTQ	1I2X	1AIE
# atoms	75	163	182	183	266	304	513	522
Index	9	10	11	12	13	14	15	16
PDB ID	1ZWF	375D	440D	4HLI	3ES0	3IM3	2IJI	1COA
# atoms	586	593	629	697	781	851	890	1057
Index	17	18	19	20	21	22	23	24
PDB ID	2AVP	1SM5	2ONT	4GSG	3ICB	1DCW	3LDE	1AYI
# atoms	1085	1137	1161	1195	1202	1257	1294	1365
Index	25	26	27	28	29	30	31	32
PDB ID	2YX5	3DFG	3LOD	1TR4	1RMP	1IF4	4DUT	3SQE
# atoms	1385	2198	2246	3423	3478	4071	4217	4647
Index	33	34	35	36	37	38		
PDB ID	1HG8	4DPF	3FR0	2H8H	2CEK	1IL5		
# atoms	4960	5824	6952	7084	8346	8349		

PQR files for each test biomolecule using PDB2PQR³⁶ with the CHARMM force field and water molecules removed.

The MSMS triangulations were generated using density values $d = 1, 2, 4, 8, 16$ and the NanoShaper triangulations were generated using scaling parameter values $s = 1, 2, 3, 4, 5$. For all surfaces a probe radius of 1.4 \AA was used.

The physical parameter values were ionic concentration $I_s = 0.15 \text{ M}$, temperature $T = 300 \text{ K}$, and solute and solvent dielectric constants $\epsilon_1 = 1$, $\epsilon_2 = 80$. The treecode parameters were multipole acceptance criterion $\theta = 0.8$, Taylor series order $p = 3$, and maximum number of particles in a leaf $N_0 = 500$. The GMRES tolerance was $1\text{E-}4$, with 10 iterations between restarts and maximum number of iterations 110.

All computations were performed in serial on the University of Michigan FLUX cluster,

with Intel Xeon CPUs running at either 2.5 or 2.8 GHz. In this system the exact processors could not be specified, so the timing results were averaged over multiple runs. The code was compiled with gfortran using the -O2 optimization flag. The newest version of the TABI-PB solver is available on GitHub at github.com/Treecodes/TABI-PB. The version of the TABI-PB solver used in this work is available on GitHub at github.com/lwwilson/TABI-PB. We also note here that TABI-PB was recently implemented as an option in the APBS package developed at Pacific Northwest National Laboratory³⁷.

RESULTS AND DISCUSSION

We first study geometric features of the surface triangulations by considering the triangle size, shape, and aspect ratio, and qualitatively comparing the generated surface meshes. We then extrapolate with respect to the number of triangles to calculate highly accurate converged values of the surface area and solvation energy; the converged result is the y -intercept of a simple extrapolation of the computed surface area or solvation energy versus N^{-1} for the two highest resolution meshes produced by MSMS and NanoShaper. For some values of the density parameter d , MSMS produced spurious results for the larger molecules or failed to even produce a triangulation at all, as observed by previous investigators²⁹; in these cases the extrapolation used the highest resolution meshes for which MSMS did not fail.

Triangulation Filter

Both MSMS and NanoShaper produce a number of small or thin triangles which reduce the computational accuracy and efficiency, and it is common practice to delete them from the simulations. Hence in the present work, triangles are deleted if their area is less than $1e-5 \text{ \AA}^2$ or if the distance between the centroids of two neighboring triangles is less than $1e-5 \text{ \AA}$. Table 2 gives the percent of deleted triangles averaged over all triangulations using MSMS and NanoShaper. Among the deleted triangles, some had area less than machine precision and these are designated as zero-area triangles. With MSMS the deleted triangles

are 0.064% of the total, while with NanoShaper the total is more than 100 times smaller. Table 2 also shows that most of the deleted MSMS triangles were zero-area, while none of this type were produced by NanoShaper.

Table 2: Triangulation filter results showing percent of deleted triangles and zero-area triangles, values shown are averaged over all triangulations using MSMS and NanoShaper, zero-area triangles are a subset of deleted triangles.

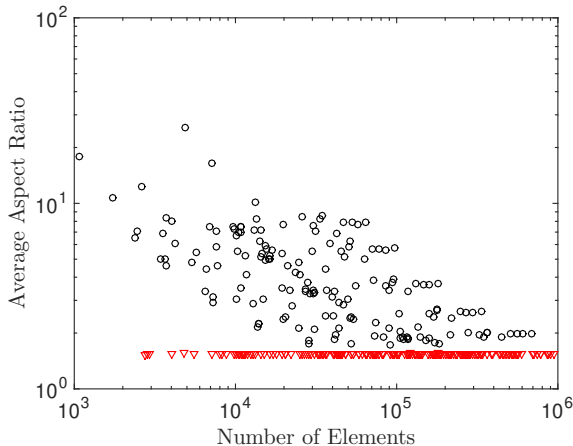
code	deleted triangles	zero-area triangles
MSMS	6.4e-2 %	5.4e-2 %
NanoShaper	5.2e-4 %	0.0e-0 %

Triangle Aspect Ratios

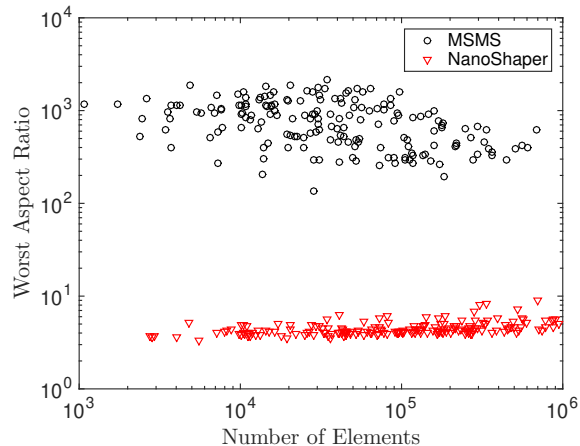
Even after filtering the triangulation as above, the aspect ratio of the remaining triangles can affect the computational performance. The aspect ratio of a triangular surface element is defined as the ratio of the longest to shortest sides. Figure 2 displays the (a) average aspect ratio, r_{avg} , and (b) maximum aspect ratio, r_{max} , versus the number of triangles, N , for each triangulation, where N varies from approximately $1e+3$ to $1e+6$, for the chosen density and scaling parameters. Figure 2a shows that the average aspect ratio of MSMS triangles is as large as $r_{avg} \approx 30$ for small N and decreases to approximately $r_{avg} \approx 2$ for large N , while the average aspect ratio of NanoShaper triangles is closer to $r_{avg} \approx 1$ for all N . Figure 2b shows that the maximum aspect ratio of MSMS triangles varies between approximately $1e+2$ and $2e+3$, while the maximum aspect ratio of NanoShaper triangles is below $1e+1$ across all triangulations.

Surface Mesh Features

Figure 3 displays the triangulation and surface potential for a representative protein (1AIE) using (a) MSMS and (b) NanoShaper with similar resolution, $N \approx 3e+4$ triangles in each



(a) average aspect ratio, r_{avg}



(b) maximum aspect ratio, r_{max}

Figure 2: Triangle aspect ratio versus number of elements N for each generated surface, (a) average aspect ratio, r_{avg} , (b) maximum aspect ratio, r_{max} , MSMS (\circ , black), NanoShaper (∇ , red).

case. The surfaces are similar at first glance, although the NanoShaper surface appears slightly smoother than the MSMS surface. Figure 4 displays a zoom of the triangulations, where several irregular features are highlighted; in the MSMS mesh, green boxes enclose *stitches* formed by high aspect ratio triangles, and a white box encloses a *cusp* formed by neighboring triangles that meet at a acute angle, while in the NanoShaper mesh, a yellow box encloses a possible irregular feature, which could in fact simply be an artifact of the surface lighting. It should be noted that irregular features are present in the MSMS mesh even after filtering; by contrast, the NanoShaper mesh is relatively free of such irregular features. The irregular features diminish the efficiency of the calculations; as shown below, calculations using MSMS meshes require more iterations to converge in comparison with calculations using NanoShaper meshes.

Dependence of S_a and E_{sol} on Mesh Resolution

In this section we examine the dependence of the surface area S_a and solvation energy E_{sol} on the mesh resolution for four representative proteins (1AIE, 1HG8, 3FR0, 1IL5). Figure 5 plots S_a and Fig. 6 plots E_{sol} versus N^{-1} , where N is the number of surface elements. As

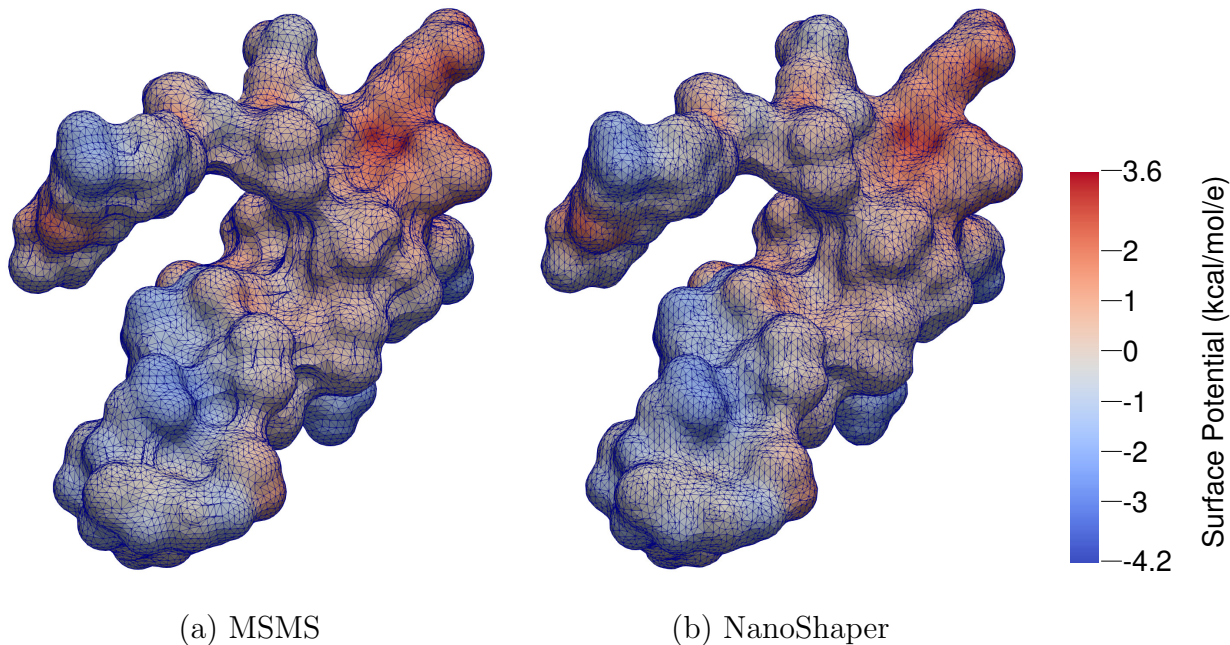
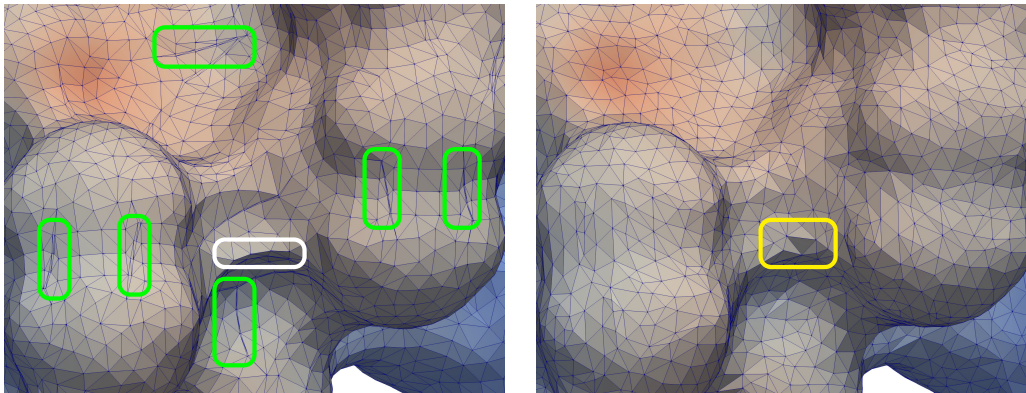


Figure 3: Protein 1AIE, SES triangulation and electrostatic potential, (a) MSMS, density $d = 6$, $N = 31480$ triangles, (b) NanoShaper, scaling parameter $s = 2$, $N = 32208$ triangles.

expected the MSMS and NanoShaper results for S_a and E_{sol} converge to similar limits since both codes approximate the solvent excluded surface, but several differences can be seen in their dependence on N .

First, concerning the surface area in Fig. 5, the MSMS and NanoShaper results converge to almost the same values in Fig. 5a,d (1AIE, 1IL5), but in Fig. 5b,c (1HG8, 3FR0), the NanoShaper surface area is 2-3% larger than the MSMS surface area. In all cases the convergence with N^{-1} is smooth. The MSMS results approach their limit somewhat faster, although MSMS was unable to generate reliable meshes with larger values of N ; either it fails to produce a mesh, or the generated mesh was poorly formed. The largest value we obtained using MSMS was $N \approx 2e+6$, whereas NanoShaper had no such limitation. Hence if it is necessary to generate a very dense mesh, or even a less dense mesh for a biomolecule with a large surface area, then NanoShaper has an advantage.

Second, concerning the solvation energy in Fig. 6, the MSMS and NanoShaper results converge to almost the same value. The MSMS results again approach their limiting value



(a) MSMS, zoomed

(b) NanoShaper, zoomed

Figure 4: Protein 1AIE, zoom of SES triangulation, (a) MSMS, density $d = 6$, $N = 31480$ triangles, green boxes enclose *stitches* formed by high aspect ratio triangles, white box encloses a *cusp* formed by neighboring triangles that meet at an acute angle, (b) NanoShaper, scaling parameter $s = 2$, $N = 32208$ triangles, yellow box encloses a possible irregular feature.

somewhat faster than the NanoShaper results, although the NanoShaper dependence on N is smoother than the MSMS dependence.

Figure 7 displays the (a) surface area S_a and (b) solvation energy E_{sol} for the entire set of 38 biomolecules, where the NanoShaper results are plotted versus MSMS results. In this case to reduce the dependence of the computed values on the mesh resolution N , we extrapolated the computed S_a and E_{sol} to the limit $N \rightarrow \infty$ using the two highest resolution meshes, density $d = 8, 16$ for MSMS and scaling factor $s = 4, 5$ for NanoShaper. The correspondence between MSMS and NanoShaper results in Fig. 7 is very good, except for two molecules, 1I2X and 375D, which consist of multiple domains, for which MSMS did not generate an accurate mesh. These two anomalous cases are indicated by the two markers furthest away from the diagonal line in Figs. 7a,b. In addition, MSMS failed to produce surfaces for 13 other runs, and produced highly distorted surfaces with spurious solvation energy for 3 more runs. These 16 spurious runs were removed from the calculations in this section. By contrast, NanoShaper failed in only one case, a low resolution mesh with scaling factor $s = 1$ for the smallest molecule in the test set (2LWC, 75 atoms).

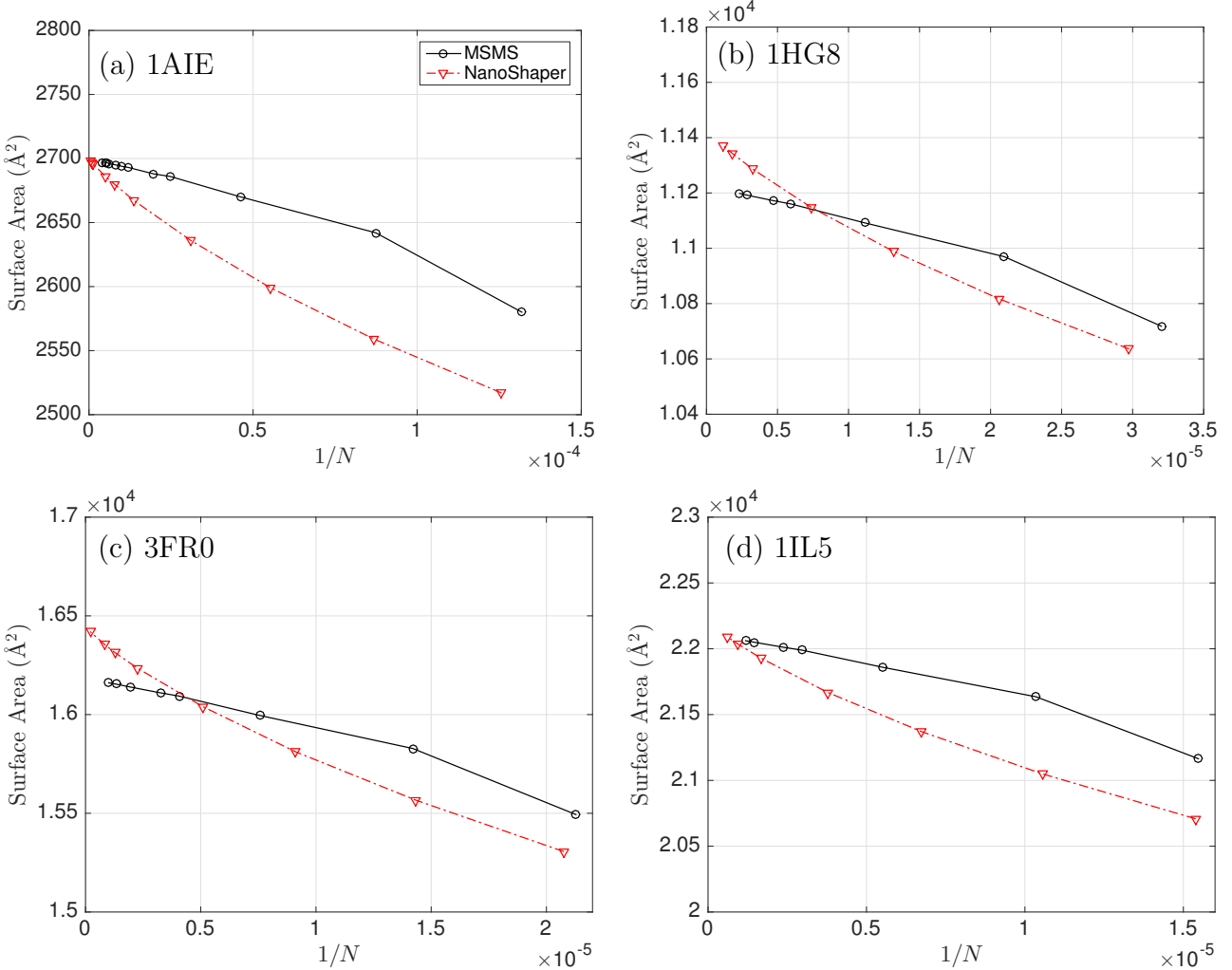


Figure 5: Surface area S_a versus N^{-1} for four representative proteins, where N is the number of triangles, MSMS (black, solid line, \circ), NanoShaper (red, dashed line, ∇).

Computational Efficiency

Figure 8a displays the total TABI-PB run time versus the number of triangles N for computing the solvation energy E_{sol} using MSMS and NanoShaper meshes, where the solid lines are least squares fits to the data. The run time for creating and filtering the meshes is less than eight seconds in all cases, and thus constitutes a negligible fraction of the total run time. The results show that in general, NanoShaper meshes require less run time than MSMS meshes. This is supported by Fig. 8b showing the number of GMRES iterations in each case, where the maximum number of iterations was set to 110. The results show that in general,

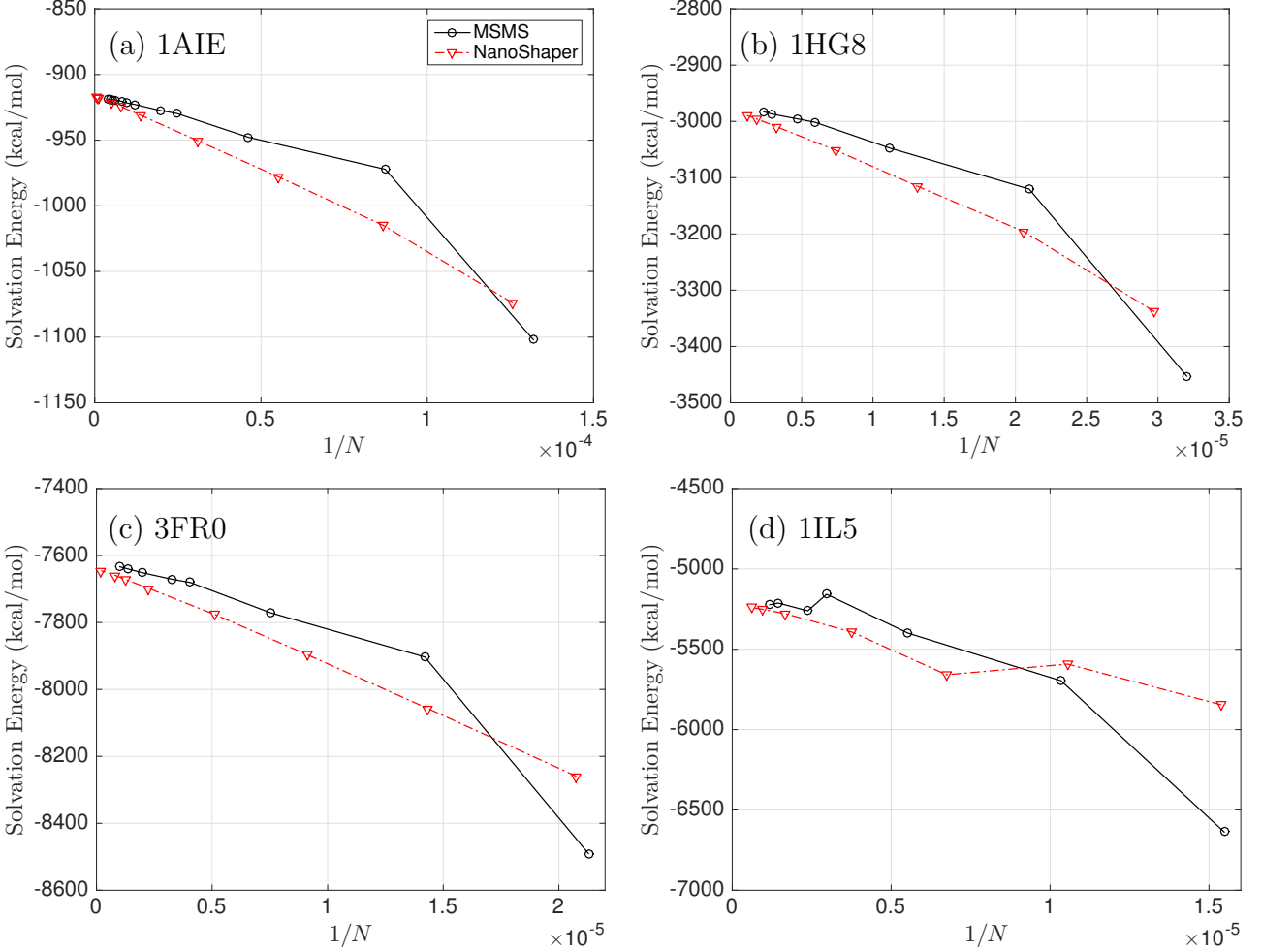


Figure 6: Solvation energy E_{sol} versus N^{-1} for four representative proteins, where N is the number of triangles, MSMS (black, solid line, \circ), NanoShaper (red, dashed line, ∇).

NanoShaper meshes require fewer GMRES iterations than MSMS meshes. Moreover, in the case of MSMS, the iteration limit was reached in 23 out of 177 meshes, while in the case of NanoShaper, the iteration limit was never reached.

Table 3 displays the average run time and average number of GMRES iterations per triangle for each mesh type over the entire set of 38 biomolecules. The results show that NanoShaper meshes require about 2/3 of the run time and 1/4 of the number of iterations required by MSMS meshes. The larger number of GMRES iterations required for MSMS meshes is attributed to the presence of triangles with large aspect ratio, as seen in Fig. 2, and irregular features in the generated surfaces, as seen in Fig. 4.

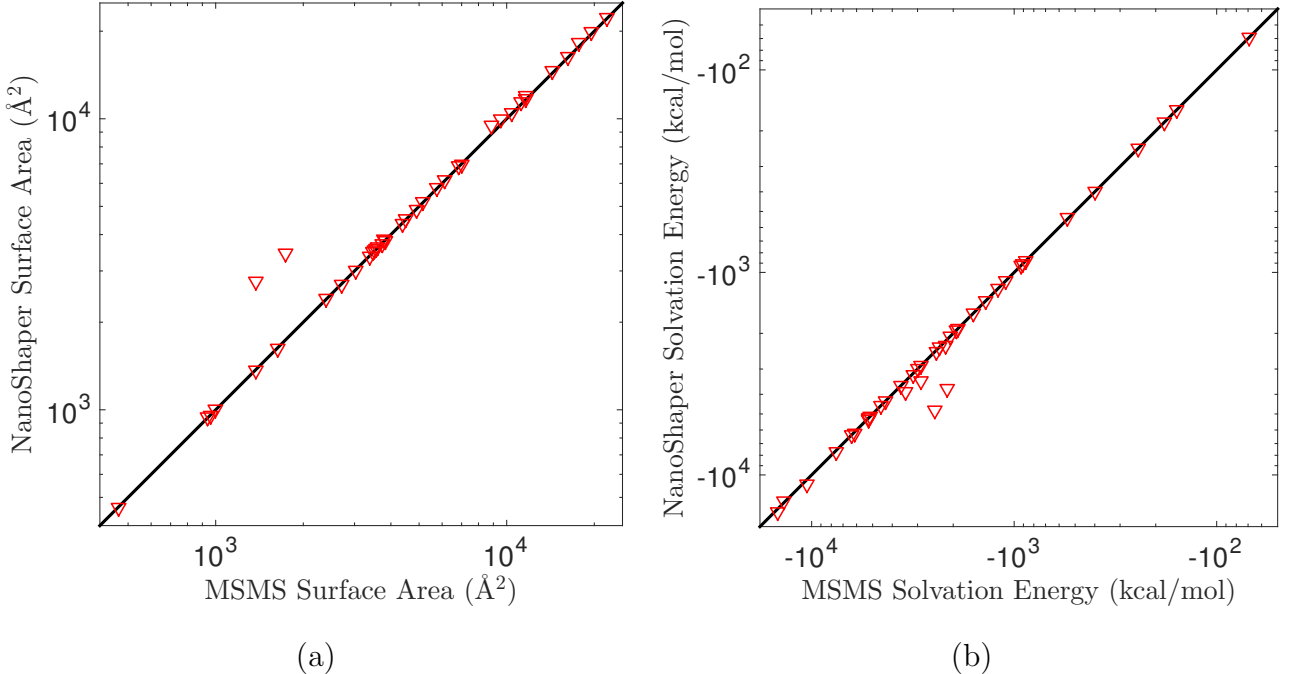


Figure 7: NanoShaper versus MSMS results for entire set of 38 biomolecules using values extrapolated to the limit $N \rightarrow \infty$, (a) surface area S_a , (b) solvation energy E_{sol} , black lines indicate perfect correspondence.

CONCLUSIONS

We compared the performance of MSMS and NanoShaper, two widely used codes for triangulating the solvent excluded surface (SES) in Poisson–Boltzmann simulations of solvated biomolecules. Comparisons were made of the surface area and electrostatic solvation energy, where the latter calculations were performed using the treecode-accelerated boundary integral (TABI-PB) solver which utilizes a well-conditioned boundary integral formulation and

Table 3: Average run time (s) and average number of GMRES iterations per triangle for MSMS and NanoShaper meshes over entire set of 38 biomolecules.

	average run time (s)/triangle	average iterations/triangle
MSMS	6.67e−3	1.17e−3
NanoShaper	4.19e−3	2.92e−4

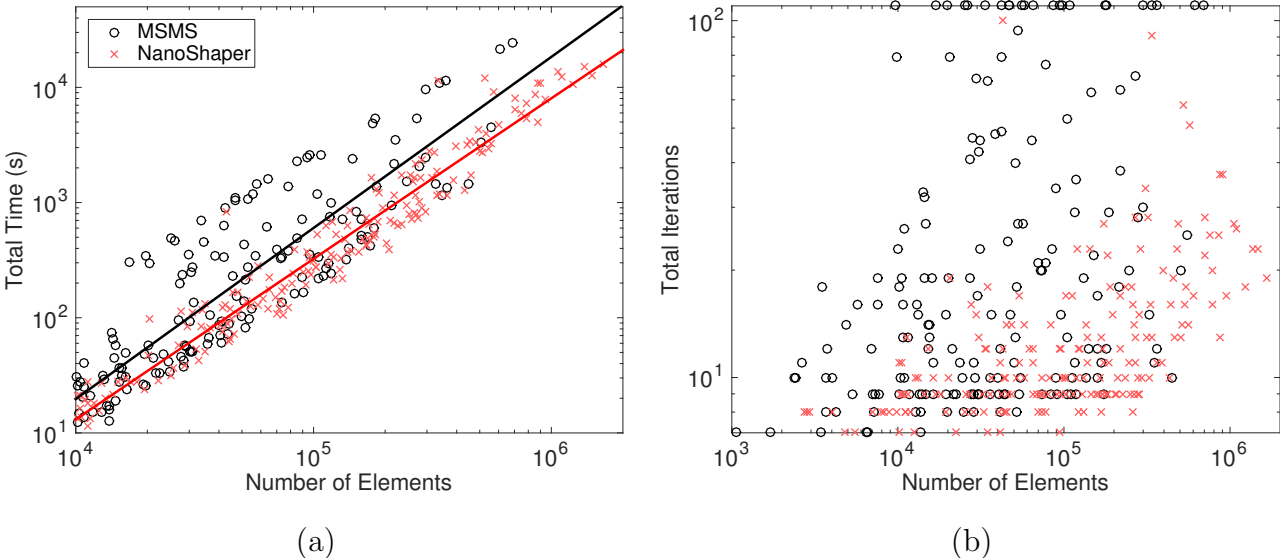


Figure 8: Computational efficiency, total run time of TABI-PB for computing solvation energy E_{sol} using MSMS (o, black) and NanoShaper (x, red) versus number of triangles N , (a) run time (s), solid lines are least squares fits, (b) number of GMRES iterations (maximum 110).

centroid collocation on the SES triangulation. In these calculations, the linear system for the electrostatic potential and its normal derivative on the SES is solved by GMRES iteration. The matrix-vector product in each step of GMRES is computed by a treecode which reduces the computational cost from $O(N^2)$ to $O(N \log N)$, where N is the number of elements in the surface triangulation.

The MSMS and NanoShaper codes were compared for a test set of 38 biomolecules. The meshes produced by the two codes are qualitatively similar, although the MSMS meshes often contained triangles of exceedingly small area and high aspect ratio. The computed values of the surface area and solvation energy produced by MSMS and NanoShaper meshes often agree to within several percent. NanoShaper meshes were more computationally efficient, requiring less run time and fewer GMRES iterations than MSMS meshes. Furthermore, NanoShaper was consistently able to produce higher resolution meshes than MSMS, and NanoShaper solvation energies exhibited smoother convergence with increasing mesh resolution. A version of TABI-PB using NanoShaper was recently implemented as an option in APBS³⁷.

ACKNOWLEDGMENTS

This work was supported by NSF grant DMS-1819094 and a catalyst grant from the Michigan Institute for Computational Discovery and Engineering (MICDE). Leighton Wilson was supported by the Department of Defense (DoD) through the National Defense Science & Engineering Graduate Fellowship (NDSEG) Program.

References

1. B. Roux and T. Simonson, *Biophys. Chem.* **78**, 1 (1999).
2. Z. Zhang, S. Witham, and E. Alexov, *Phys. Biol.* **8**, 035001 (2011).
3. J. Tomasi, *Theor. Chem. Acc.* **112**, 184 (2004).
4. N. A. Baker, in *Numerical Computer Methods, Part D*, edited by L. Brand and M. L. Johnson (Academic Press, 2004), vol. 383 of *Methods in Enzymology*, chap. 5, pp. 94–118, 1st ed.
5. B. Lu, Y. C. Zhou, M. J. Holst, and J. A. McCammon, *Commun. Comput. Phys.* **3**, 973 (2008).
6. M. J. Holst and F. Saied, *J. Comput. Chem.* **16**, 337 (1995).
7. N. A. Baker, D. Sept, S. Joseph, M. J. Holst, and J. A. McCammon, *Proc. Natl. Acad. Sci. U.S.A.* **98**, 10037 (2001).
8. R. Luo, L. David, and M. K. Gilson, *J. Comput. Chem.* **23**, 1244 (2002).
9. J. Wang and R. Luo, *J. Comput. Chem.* **31**, 1689 (2010).
10. D. Chen, Z. Chen, C. Chen, W. Geng, and G. W. Wei, *J. Comput. Chem.* **32**, 756 (2011).
11. A. H. Boschitsch and M. O. Fenley, *J. Chem. Theory Comput.* **7**, 1524 (2011).
12. W. Geng and S. Zhao, *Mol. Based Math. Biol.* **1**, 109 (2012).
13. L. Wilson and S. Zhao, *Int. J. Numer. Anal. Model.* **13**, 852 (2016).
14. M. J. Holst, N. A. Baker, and F. Wang, *J. Comput. Chem.* **21**, 1319 (2000).
15. N. A. Baker, M. J. Holst, and F. Wang, *J. Comput. Chem.* **21**, 1343 (2000).
16. J. Liang and S. Subramaniam, *Biophys. J.* **73**, 1830 (1997).

17. A. H. Juffer, E. F. F. Botta, B. A. M. van Keulen, A. van der Ploeg, and H. J. C. Berendsen, *J. Comput. Phys.* **97**, 144 (1991).
18. A. H. Boschitsch, M. O. Fenley, and H.-X. Zhou, *J. Phys. Chem. B* **106**, 2741 (2002).
19. W. Geng and R. Krasny, *J. Comput. Phys.* **247**, 62 (2013).
20. C. D. Cooper, J. P. Bardhan, and L. A. Barba, *Comput. Phys. Commun.* **185**, 720 (2014).
21. M. Chen and B. Lu, *J. Chem. Theory Comput.* **7**, 203 (2011).
22. S. Decherchi and W. Rocchia, *PLoS ONE* **8**, e59744 (2013).
23. F. M. Richards, *Annu. Rev. Biophys. Bioeng.* **6**, 151 (1977).
24. M. L. Connolly, *J. Appl. Crystallogr.* **18**, 499 (1985).
25. W. Rocchia, S. Sridharan, A. Nicholls, E. G. Alexov, A. Chiabrera, and B. Honig, *J. Comput. Chem.* **23**, 128 (2002).
26. W. Rocchia, *Math. Comput. Model.* **41**, 1109 (2005).
27. H.-L. Cheng and X. Shi, *Comput. Geom.* **42**, 192 (2009).
28. M. Chen, B. Tu, and B. Lu, *J. Mol. Graph. Model.* **38**, 411 (2012).
29. T. Can, C.-I. Chen, and Y.-F. Wang, *J. Mol. Graph. Model.* **25**, 442– (2006).
30. R. Egan and F. Gibou, *J. Comput. Phys.* **374**, 91 (2018).
31. M. F. Sanner, A. J. Olson, and J.-C. Spohner, in *Proceedings of the 11th ACM Symposium on Comput. Geom.* (Association for Computing Machinery, 1995), pp. C6–C7.
32. D. Xu and Y. Zhang, *PLoS ONE* **4**, e8140 (2009).
33. D. Xu, H. Li, and Y. Zhang, *J. Comput. Biol.* **20**, 805 (2013).
34. S. Decherchi, J. Colmenares, C. E. Catalano, M. Spagnuolo, E. Alexov, and W. Rocchia, *Commun. Comput. Phys.* **13**, 61 (2013).

35. T. Liu, M. Chen, and B. Lu, *J. Mol. Model.* **21**, 113 (2015).
36. T. J. Dolinsky, J. E. Nielsen, J. A. McCammon, and N. A. Baker, *Nucleic Acids Res.* **32**, W665 (2004).
37. E. Jurrus, D. Engel, K. Star, K. Monson, J. Brandi, L. E. Felberg, D. H. Brookes, L. Wilson, J. Chen, K. Liles, et al., *Protein Sci.* **27**, 112 (2017).